Solution of the Euler equations around a double ellipsoïdal shape using unstructured meshes and including real gas effects

François Dubois, Olivier Michaux

Workshop on Hypersonic Flows for Reentry Problems,
Antibes (France), January, 22-25 1990.

Solution of the Euler Equations Around a Double Ellipsoidal Shape Using Unstructured Meshes and Including Real Gas Effects.

François DUBOIS and Olivier MICHAUX.
AEROSPATIALE, Division Systèmes Stratégiques et Spatiaux
Direction Technique, BP 96, F-78133 Les Mureaux Cedex, France.

Abstract

We present the numerical solution of the Euler equations of gas dynamics around the double ellipsoidal shape proposed by the organizers of the Antibes 1990 workshop. In two of the test cases we consider a modelization of air by a polytropic perfect gas, at an upstream Mach number $M_\infty = 8.15$, and under incidences $\alpha = 0°$ and $30°$ (problems 6.1.5 and 6.1.7). The last test case is related to hypersonic regimes ($M_\infty = 25$, $\alpha = 30°$) and the air is therefore described as a real gas at chemical equilibrium (problem 6.3.9).

In the first part of this paper we describe our three-dimensional Euler computing code named CEL3GR developed at AEROSPATIALE Les Mureaux since 1987. In the second part, we present the generation of our two box mesh around the double ellipsoid and we emphasize on the approximation of the nontrivial line of intersection. The third part is devoted to the numerical results for each test case.

I. Description of the Euler Solver CEL3GR.

The code CEL3GR is based on the MUSCL scheme (second order accurate upstream scheme) proposed initially by Van Leer [1979] and the use of finite element type unstructured meshes. It has been developed at the Technical Direction of the Space and Strategic Systems Division of AEROSPATIALE since 1987. We refer to Mercier [1987] for a preliminary 2D version, to Michaux [1989] for the 3D version and to Pollet-Brenner [1989] for internal aerodynamics applications including a moving body.

The computational domain is divided into finite volumes K that are supposed to satisfy the usual restrictions associated with finite element meshes (see Ciarlet

This contribution has been published in *Hypersonic Flows for Reentry Problems, Volume II: Test Cases – Experiments and Computations Proceedings of a Workshop Held in Antibes, France, 22–25 January 1990*, Editors Jean-Antoine Désidéri, Roland Glowinski, Jacques Périaux, Springer Verlag, pages 358-373, 1992. Edition January 2024.

Workshop on Hypersonic Flows for Reentry Problems,
Antibes (France), January, 22-25 1990.

Solution of the Euler Equations Around a Double Ellipsoidal Shape Using Unstructured Meshes and Including Real Gas Effects.

François DUBOIS and Olivier MICHAUX.
AEROSPATIALE, Division Systèmes Stratégiques et Spatiaux
Direction Technique, BP 96, F-78133 Les Mureaux Cedex, France.

Abstract

We present the numerical solution of the Euler equations of gas dynamics around the double ellipsoidal shape proposed by the organizers of the Antibes 1990 workshop. In two of the test cases we consider a modelization of air by a polytropic perfect gas, at an upstream Mach number $M_\infty = 8.15$, and under incidences $\alpha = 0°$ and 30° (problems 6.1.5 and 6.1.7). The last test case is related to hypersonic regimes ($M_\infty = 25$, $\alpha = 30°$) and the air is therefore described as a real gas at chemical equilibrium (problem 6.3.9).

In the first part of this paper we describe our three-dimensional Euler computing code named CEL3GR developed at AEROSPATIALE Les Mureaux since 1987. In the second part, we present the generation of our two box mesh around the double ellipsoid and we emphasize on the approximation of the nontrivial line of intersection. The third part is devoted to the numerical results for each test case.

I. Description of the Euler Solver CEL3GR.

The code CEL3GR is based on the MUSCL scheme (second order accurate upstream scheme) proposed initially by Van Leer [1979] and the use of finite element type unstructured meshes. It has been developed at the Technical Direction of the Space and Strategic Systems Division of AEROSPATIALE since 1987. We refer to Mercier [1987] for a preliminary 2D version, to Michaux [1989] for the 3D version and to Pollet-Brenner [1989] for internal aerodynamics applications including a moving body.

The computational domain is divided into finite volumes K that are supposed to satisfy the usual restrictions associated with finite element meshes (see Ciarlet

[1976]). Moreover, we restrict ourselves in the present version to finite volumes that are hexahedrons or prisms. As usual with the finite volume method, we integrate the Euler equations (for details concerning this classical model and notations we refer to Landau-Lifchitz [1953]) on each cell K and derive in this way a system of ordinary differential equations for the mean values of the conservative variables in the control volume K:

$$(1) \qquad \frac{dU_K}{dt} + \frac{1}{|K|} \sum_{f \subset \partial K} \text{area}(f) \cdot \phi(f) = 0 \ .$$

where ∂K denotes the boundary of K, f a generic face of ∂K and $|K|$ the measure of the cell K. The numerical flux $\phi(f)$ is computed according to the **second order accurate** MUSCL approach that can be divided into three steps: (i) evaluation of the gradient of density, momentum and volumic internal energy in each cell K, (ii) nonlinear extrapolation of these fields on the two sides of each interface f in order to respect monotonicity constraints and (iii) approximate solution of the Riemann problem at each face in the way initially proposed by Godunov [1959]. The assumption of an unstructured mesh makes the first step not so obvious. We compute the three components of the mean value of the gradient $\nabla\varphi(K)$ in the cell K of a scalar field φ according to Green's formula:

$$(2) \qquad \nabla\varphi(K) = \frac{1}{|K|} \int_{\partial K} \varphi \, n \, d\gamma \ .$$

Therefore it is sufficient to interpolate φ on each face f from the cell values $\varphi(K)$ in a centered way to achieve this first step. The nonlinear extrapolation (second step) $\varphi(K,f)$ of the field φ on the face f on the side of the element K generalizes the procedure introduced by Van Leer [1977] ; we suppose that the field φ is **polynomial of degree 1** between the centers x(K) of the cell and x(f) of the face and we limit the extrapolation associated with the first order Taylor formula by some parameter $\alpha(K,\varphi)$ between 0 and 1. We obtain :

$$(3) \qquad \varphi(K,f) = \varphi(K) + \alpha(K,\varphi) \cdot \nabla\varphi(K) \cdot (x(f) - x(K)) .$$

and $\alpha(K,\varphi)$ is chosen as close to 1 as possible in order to satisfy the following monotonicity condition

$$(4) \qquad \min_{\text{L neighbouring K}} \varphi(L) \;\le\; \varphi(K,f) \;\le\; \max_{\text{L neighbouring K}} \varphi(L) \quad ,$$

for each face f of the element K.

From the five scalar parameters $\varphi(K,f)$ (i.e. one for density, three for momentum and one for volumic internal energy) we easily obtain an extrapolation of the conservative variables U(K,f). The third step is strongly nonlinear and evaluates the flux at the interface f that results from the interface Riemann problem. The data of this one-dimensional discontinuity decomposition are the two values $\varphi(L,f)$ and $\varphi(R,f)$ and the direction of propagation is the normal n(f) of the interface. We have chosen the flux splitting ψ proposed by Sanders-Prendergast [1974] which has the advantage of being parameterized **only** by the following two thermodynamics functions : the pressure and the (equilibrium) sound velocity given as functions of the density and the internal energy. In the case of a (non perfect) equilibrium air modelization, we used the function tgas1 proposed by Srinivasan et al [1987]. Then we compute the numerical flux in (1) according to the relation :

$$(5) \qquad \phi(f) \;=\; \psi\,(\,U(L,f)\,,\,n(f)\,,\,U(R,f)\,) \quad .$$

The boundary conditions are treated weakly, i.e. the external state (in the case of a fluid artificial boundary) or the mirror state (to take into account the body) is introduced on one hand in the arguments of the right hand side of relation (5) to take into account the Riemann problem at the boundary. For more details concerning the treatment of the boundary conditions in terms of fluxes and its relation with the solution of Riemann problems, we refer to Dubois-Le Floch [1989].

To obtain a steady state solution of the Euler equations the integration of the differential system (1) with respect to time is performed with a **second order accurate explicit** temporal scheme (the Courant-Friedrichs-Lewy (CFL) number is typically of the order 0.4 to 0.6 in our computations) of the predictor-corrector type with a **conservative** predictor step :

$$(6)(a) \qquad \frac{U_K^{n+1} - U_K^n}{\Delta t} + \frac{1}{|K|} \sum_{f \subset \partial K} |f| \cdot \phi(f)^{n+1/2} = 0 \quad ,$$

$$(6)(b) \qquad \frac{U_K^{n+1/2} - U_K^n}{\Delta t / 2} + \frac{1}{|K|} \sum_{f \subset \partial K} |f| \cdot \phi(f)^n = 0 \ .$$

We focus now on the multidomain treatment in the supersonic regions of the flow. We consider a **plane** surface Σ separating two domains 1 and 2 in such a way that we know **a priori** that the flow is supersonic in the direction orthogonal to Σ everywhere on Σ. Node coincidence on each side of Σ is not required by our computer code. To handle the interface conditions we proceed as follows. In domain 1, the plane Σ corresponds to a supersonic outflow and no boundary data has to be taken into account when we compute the flux (5) at this boundary. When convergence is obtained in this first domain, we know **both** the state U(f1) and the flux ϕ(f1) on each face f1 of the mesh of the domain 1 lying on Σ. We transfer the fluxes across the interface inside domain 2 by a **conservative interpolation of the fluxes** :

$$(7) \qquad \text{area (f2)} \cdot \phi_2(\text{f2}) = \sum_{\text{f1 face of domain 1 on } \Sigma} \text{area (f1} \cap \text{f2)} \cdot \phi(\text{f1}) \ ,$$

for f2 face of domain 2 on Σ .

The second order accuracy is obtained in domain 2 by using the states U(f1) given at the boundary from the first domain. This type of boundary procedure is referenced as a "given state and given flux" boundary condition.

The code has been developed and optimized on the Cray-XMP 416 of the "Club Aéronautique" located at ONERA. Due to the data structure, **all** the do-loops have been vectorized and the present version uses **39 microsecond of CPU time per cell and per time step** (in the polytropic case ; 85 μs / Δx / Δt with real gas effects) as well as 130 words per cell concerning the memory efficiency. Thus up to 100.000 cells can be introduced in the main memory of the Cray XMP.

II. Mesh Generation around the Double Ellipsoid.

The computational domain is divided into two boxes corresponding respectively to the nose region and the remaining part of the body. The plane Σ of separation is located at the abscissa $x = x^* = -0.03742$ (relatively to the coordinate system proposed by Desideri [1989]).

The mesh of the nose region ($x<x^*$) is generated by 37 half-planes turning around the Ox axis inside the region $\{y>0\}$. Each meridian section is meshed between the body and the "infinite boundary" (semi-empirically determined for each test case) by a 46x31 structured mesh . The threedimensional cells generated in this way are hexahedrons except around the x-axis where we obtain prisms.

The mesh of the second box ($x>x^*$) is obtained by a set of 46 planes of the type "x=constant" associated with a bidimensional mesh of 37x31 points in each section. From this structured set of points, we have generated a **unstructured topology** in such a way that the **intersection line** between the two ellipsoïdal shapes **is discretized by edges that belongs to the mesh** (in the finite element sense, see figure 1). In this way, the intersection line is discretized with a precision of the order $O(h^2)$ which would be only O(h) with a structured topology. For more details, we refer to Dubois [1989].

The union of these two computational domains constitutes our mesh. It contains 91 x 37 x 31 points and 97.500 elements.

III Presentation of the results.

The first case is problem **6.1.5**; the infinite Mach number is 8.15 and the incidence is 0°. Two strong shock waves are generated by the nose and the "canopy" of the double ellipsoïd. The distribution of the pressure coefficient Cp is given in figure 3. We remark that the bow shock and the canopy shock intersect (see for example the iso-Mach contours in the meridian plane $y = 0$ in figure 2) and produce a shock wave and a contact discontinuity. The latter is weak and close to the reflected bow shock wave. Due to a relative coarse mesh in this region of the flow, this contact discontinuity is only visible on the iso-density contours (figure 4). We also remark that the entropy lines in the meridian plane (figure 5) enter **into** the body. This fact indicates that the numerical entropy generated by the scheme is very low (the reverse situation, i.e. streamlines generated by the shape, is common when the numerical dissipation is more important). We also present a view of the Mach number contours on boundary surfaces of the computational domain (figure 6).

The second computation is problem **6.1.7**; the infinite Mach number is 8.15 and the incidence is 30°. The two shock waves do not intersect in this case as we can see on the iso-Mach number contours in the meridian plane (figure 7). The plane separating the two computational boxes is visible on this view ; moreover, the bow shock wave is better captured in the first box, due to a more refined mesh. The Cp

wall distribution contours (figure 8) clearly show that the canopy shock is in comparison weaker in this case than in the previous one (see figure 3). The iso-density and iso-entropy contours in the meridian plane are presented in figures 9 and 10. The streamlines on the wall (figure 11) are regular as in the previous test case.

Our third test case is problem **6.3.9**. The air is no longer a polytropic perfect gas but a real gas at chemical equilibrium. The infinite Mach number is 25 and the incidence 30°. The convergence has been obtained in two steps: we used the first order accurate scheme (in space and time) to obtain a good approximation of the solution before integrating in time with the numerical scheme described in part I and obtaining a converged result. As in the previous case, the two shock waves do not interact (see the iso-Mach number contours in the meridian plane in figure 12). We also note in the pressure (figure 13), Mach number (figure 14) and temperature distributions (figure 15) along the body the oblique shock wave and the stagnation point, particularily visible in the Mach number distribution. The transversal Mach number repartition on the body in the plane $x = 0$ (see figure 16 indicates that the canopy shock wave is quasi-transversal in this part of the flow. This last result is not clearly visible on the threedimensional views of Mach number on the boundaries (figure 17) and the streamlines on the body (figure 18).

Conclusion.

In the test cases around the double ellipsoidal shape the computing code CEL3GR developed at AEROSPATIALE DSSS (Les Mureaux) has proved its capability to solve the Euler equations of gas dynamics in supersonic and hypersonic situations. Due to the choice of an unstructured mesh, other types of geometries have also been taken into account such as transonic nozzle flows. Further developments are under study.

Acknowledgments.

We thank Eric Chaput, Jean-Jacques Chattot and Bertrand Mercier for stimulating discussions and helpful suggestions all along this work.

References.

Ciarlet P.G. **The Finite Element Method for Elliptic Problems**, North Holland, Amsterdam, 1976.

Desideri J.A. Output Formats for Presentation of Computational Results, INRIA Sophia Antipolis, June 1989.

Dubois F., Le Floch P. Boundary Conditions for Nonlinear Systems of Conservation Laws, in **Notes on Numer. Fluid Mechanics, 24,** Ballmann-Jeltsch eds, Vieweg, Braunschweig, pp. 96-104, 1989.

Dubois F. Maillage surfacique non structuré du double ellipsoïde, Internal note, Aérospatiale S/DT/MI n° 58/89, June 1989.

Godunov S.K. A finite Difference Method for the Numerical Computation of Discontinuous Solutions of the Equations of Fluid Dynamics, Math. Sb., **47,** pp. 271-290, 1959.

Landau L, Lifchitz E. **Fluid Mechanics**, Moscow 1953, Pergamon Press, Oxford, 1959.

Mercier B. Mise en oeuvre d'un schéma décentré d'ordre 2 pour les équations d'Euler instationnaires, Internal note, Aérospatiale S/DT/N n° 8/87, June 1987.

Michaux O. Computation of Hypersonic Flows with the Euler Equations Including Real Gas Effects, EUROpean MECHanics Colloquim (N 206), Torino, Italy, 3-6 April 1989.

Pollet M., Brenner P. Aerodynamics With Moving Bodies Applied to Solid Propulsion, AIAA paper n° 1989-2779, AIAA/ASME/SAE 25th Joint Propulsion Conference, Monterey, July 1989.

Sanders R.H., Prendergast K.H. The Possible Relation of 3 Kiloparsec Arm to Explosions in the Galactic Nucleus, The Astrophysical Journal, **188,** pp. 489-500, 1974.

Srinivasan S., Tannehill J.C., Weillmuenster K.J. Simplified Curve Fits for the Thermodynamic Properties of Equilibrium Air, NASA R.P. 1181, august 1987.

Van Leer B. Towards the Ultimate Conservative Scheme IV. A New Approach to Numerical Convection, J. Comp. Phys., **23,** pp. 276-299, 1977.

Van Leer B. Towards the Ultimate Conservative Scheme V. A Second Order Sequel to Godunov's Method, J. Comp. Phys., **32,** pp. 101-136, 1979.

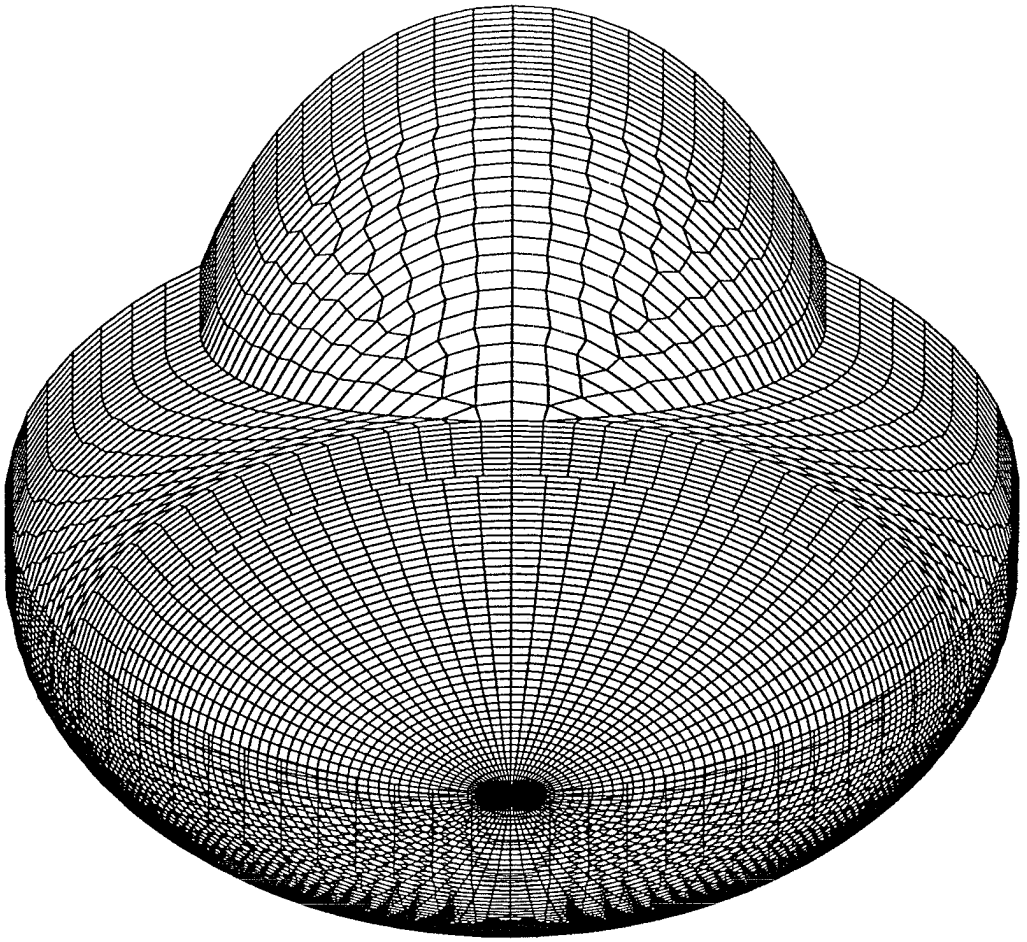

Figure 1. Unstructured mesh on the shape of the double ellipsoïd. Triangles are generated to discretize precisely the line of intersection. The limit between the two boxes without node coincidence is also clearly visible.

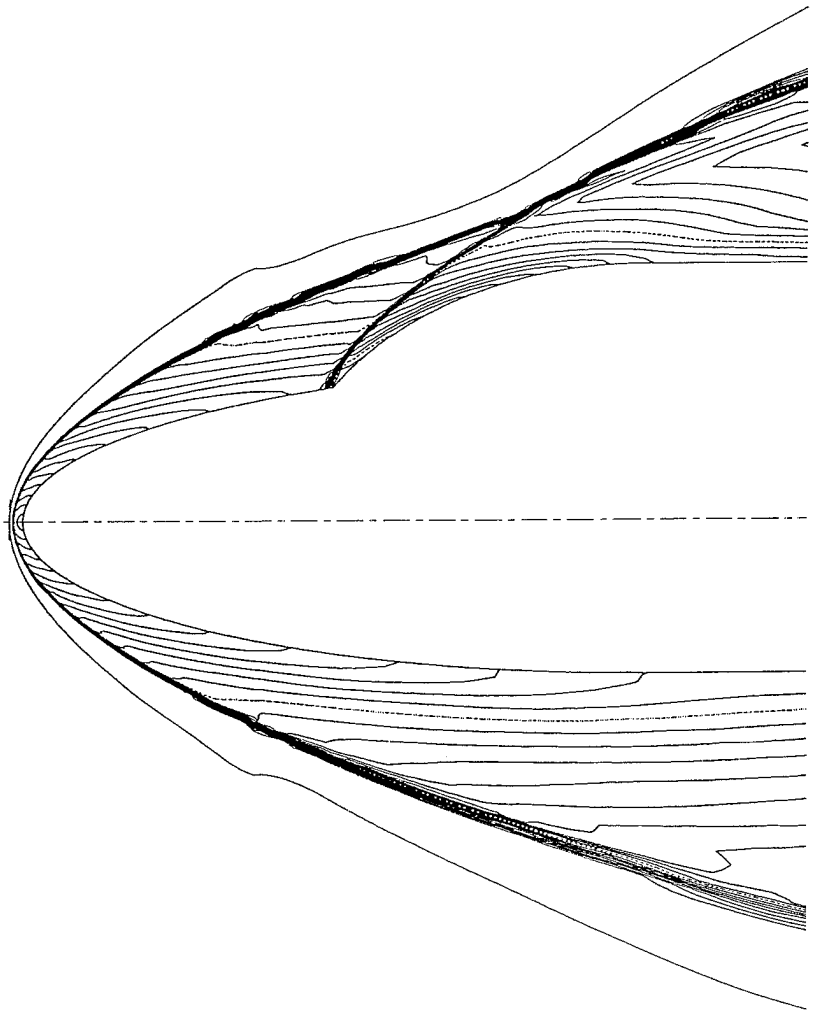

Figure 2. Problem 6.1.5, $M_\infty = 8.15$, $\alpha = 0°$. Mach number iso-value contours in the plane $y = 0$ ($\Delta m = 0.25$).

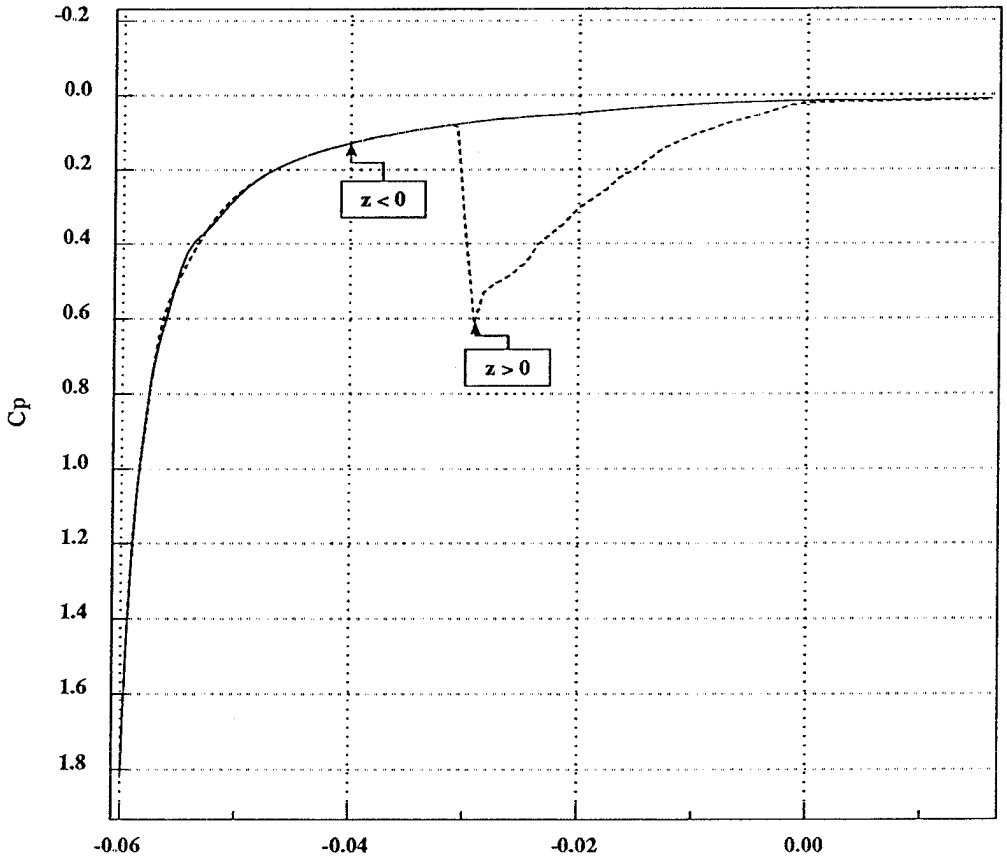

Figure 3. Problem 6.1.5, $M_\infty = 8.15$, $\alpha = 0°$. Cp wall distribution in the plane y = 0.

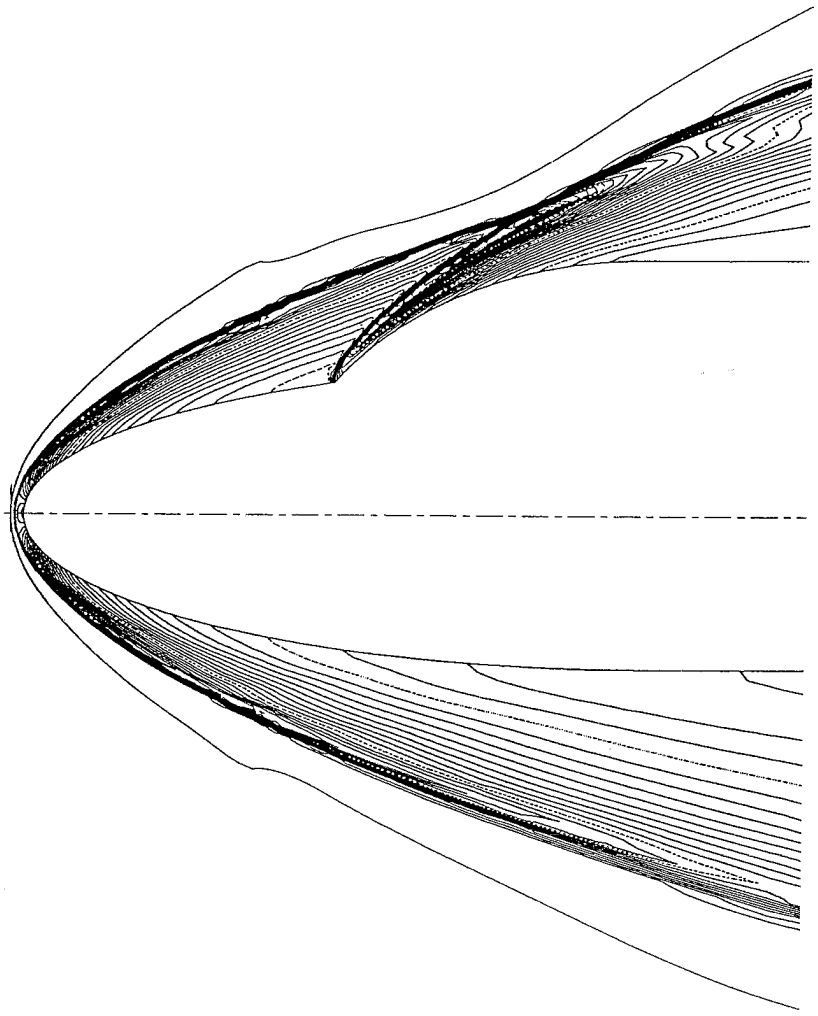

Figure 4. Problem 6.1.5, $M_\infty = 8.15$, $\alpha = 0°$. Density iso-value contours in the plane $y = 0$ ($\Delta\rho = 0.25$).

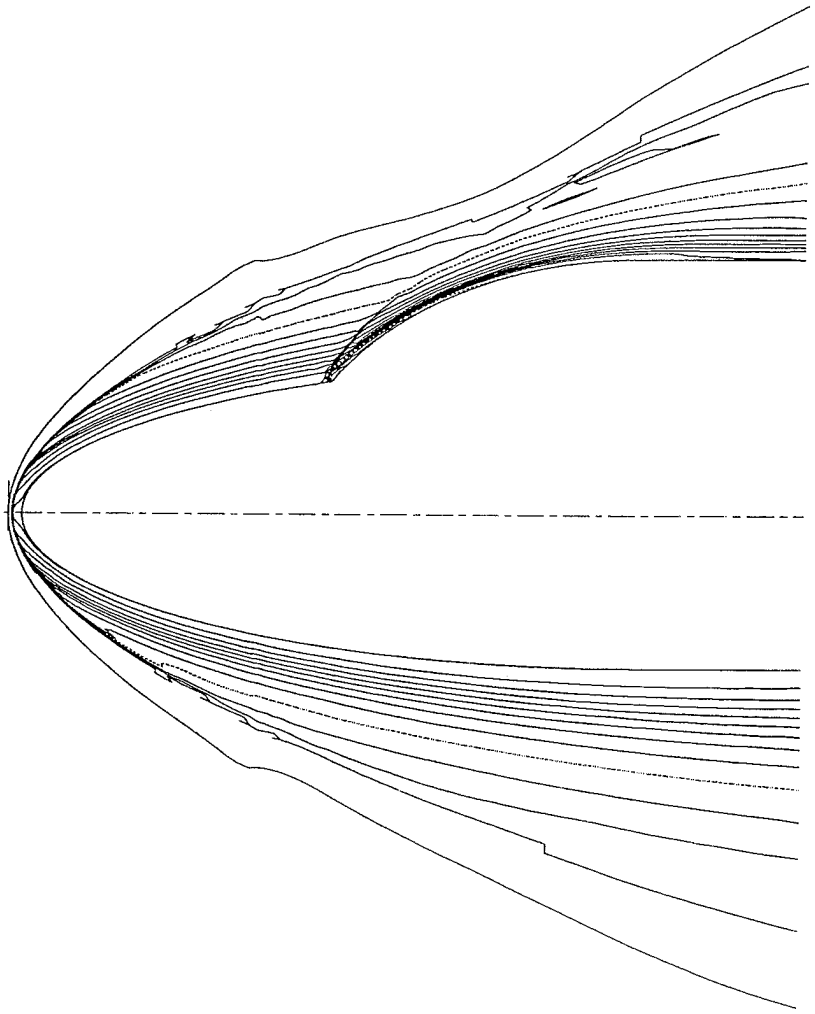

Figure 5. Problem 6.1.5, $M_\infty = 8.15$, $\alpha = 0°$. Entropy iso-value contours in the plane $y = 0$ ($\Delta s = 0.5$).

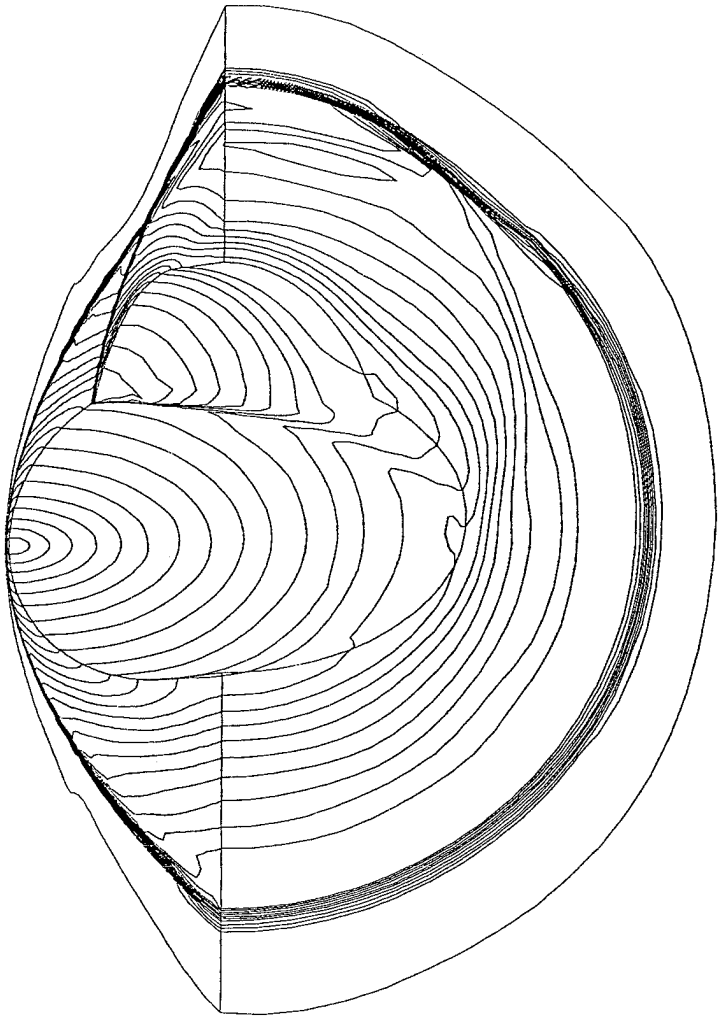

Figure 6. Problem 6.1.5, $M_\infty = 8.15$, $\alpha = 0°$. Mach number iso-value contours on the body and in the planes $y = 0$ and $x = 0.016$.

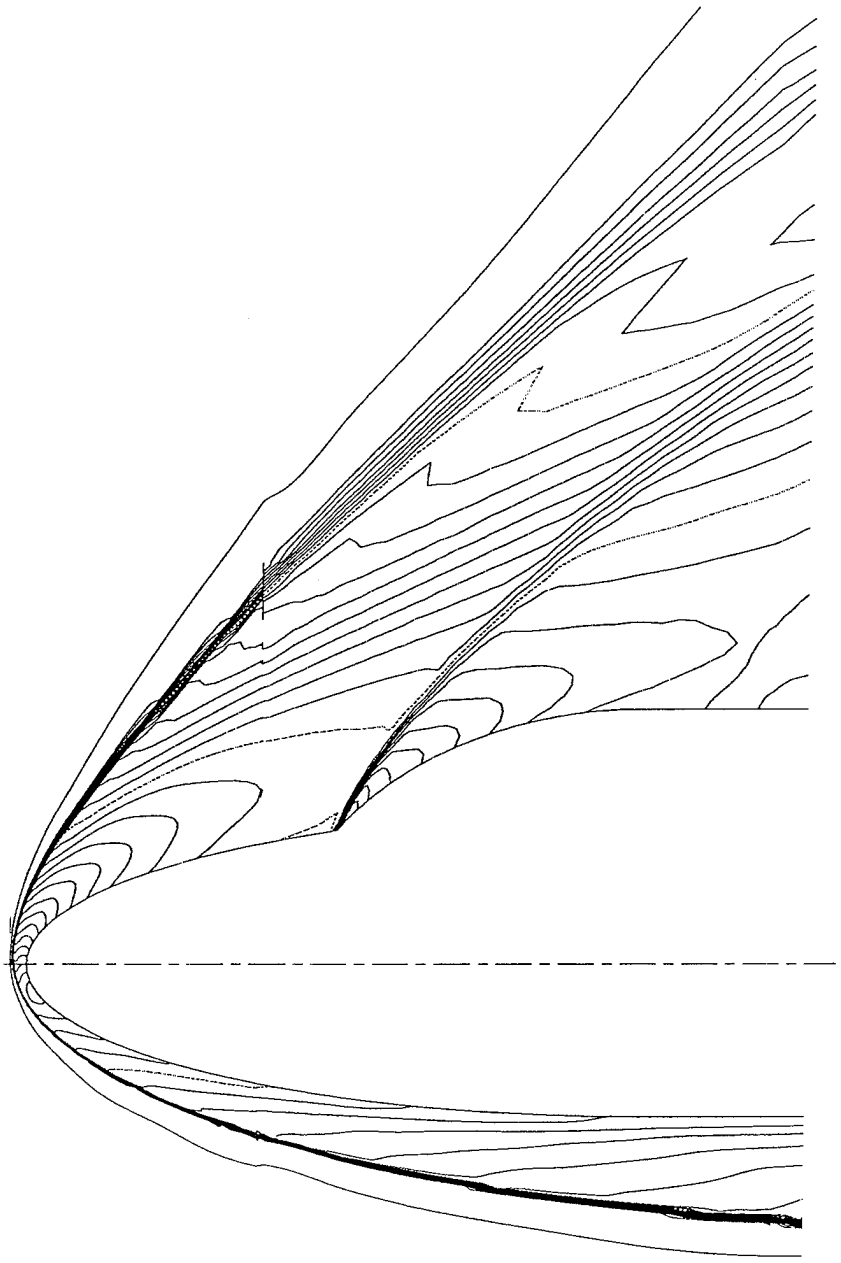

Figure 7. Problem 6.1.7, $M_\infty = 8.15$, $\alpha = 30°$. Mach number iso-value contours in the plane $y = 0$ ($\Delta m = 0.25$).

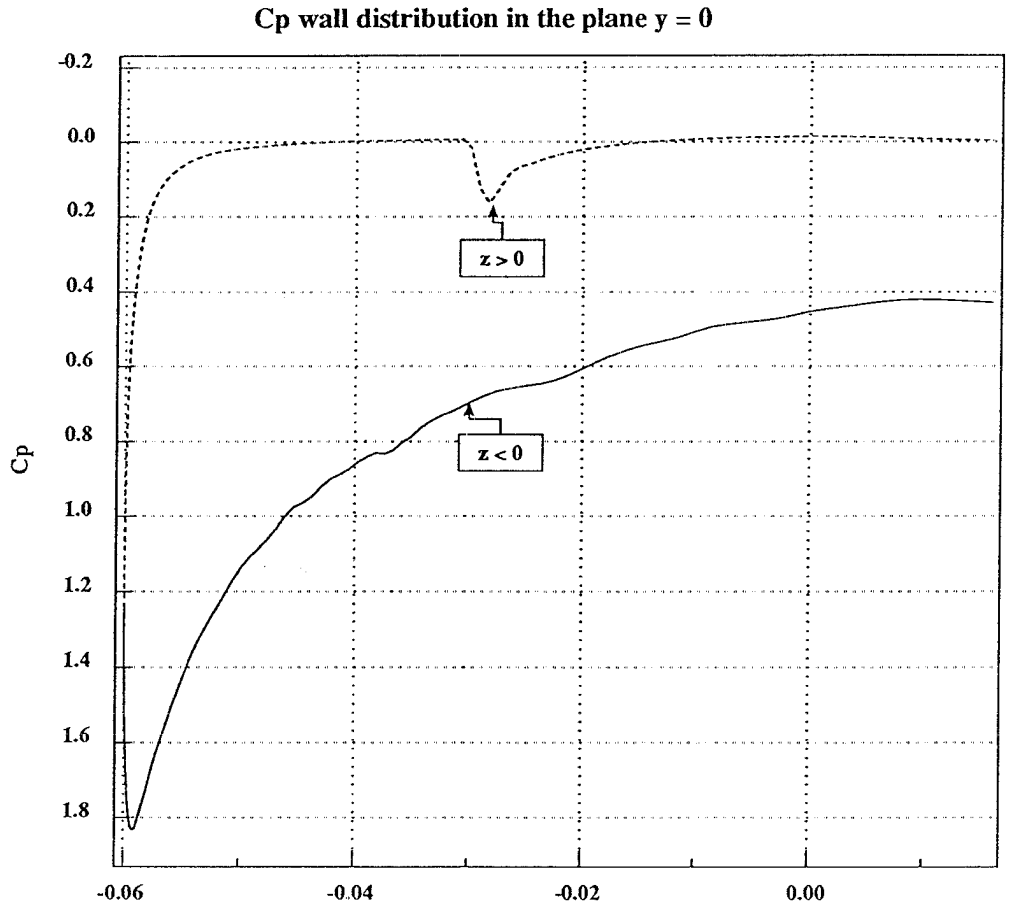

Figure 8. Problem 6.1.7, $M_\infty = 8.15$, $\alpha = 30°$. Cp wall distribution in the plane y = 0.

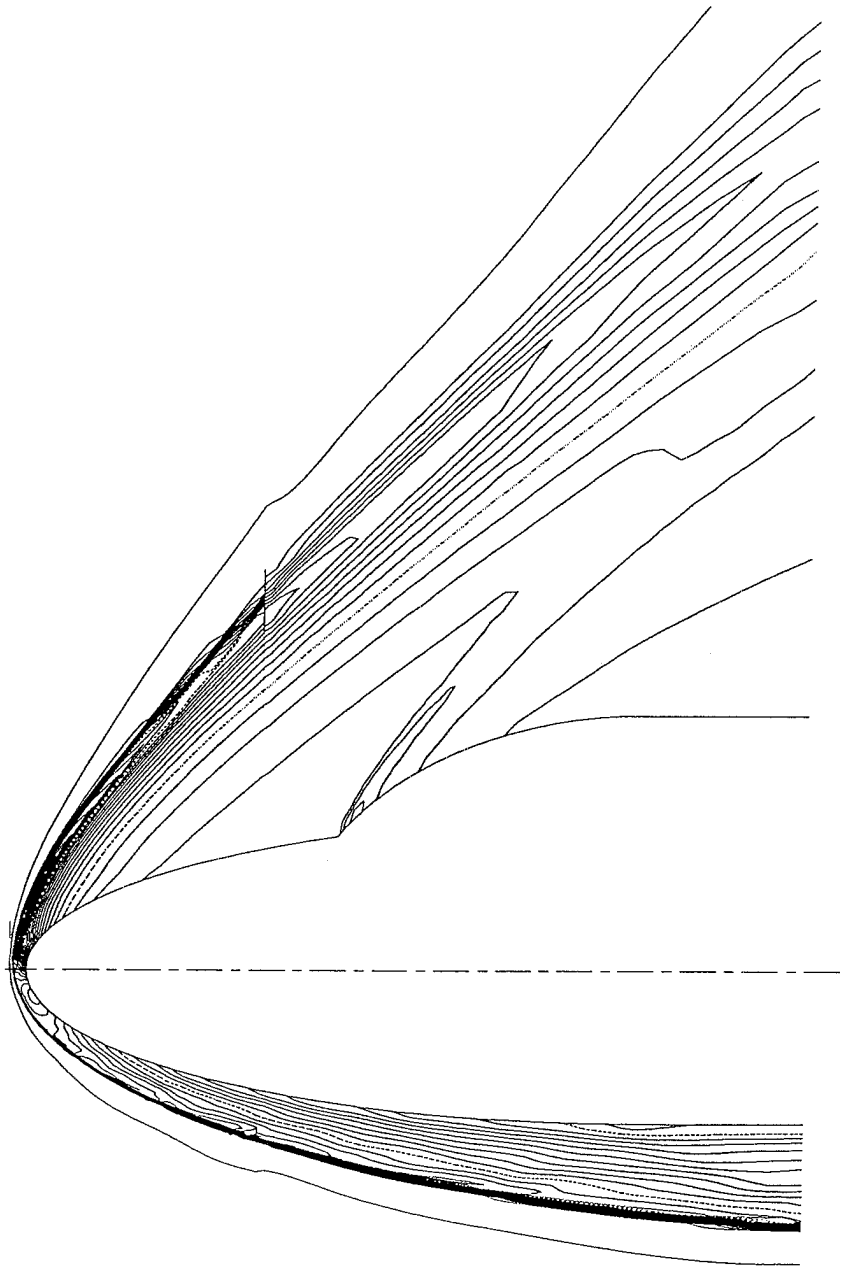

Figure 9. Problem 6.1.7, $M_\infty = 8.15$, $\alpha = 30°$. Density iso-value contours in the plane $y = 0$ ($\Delta\rho = 0.25$).

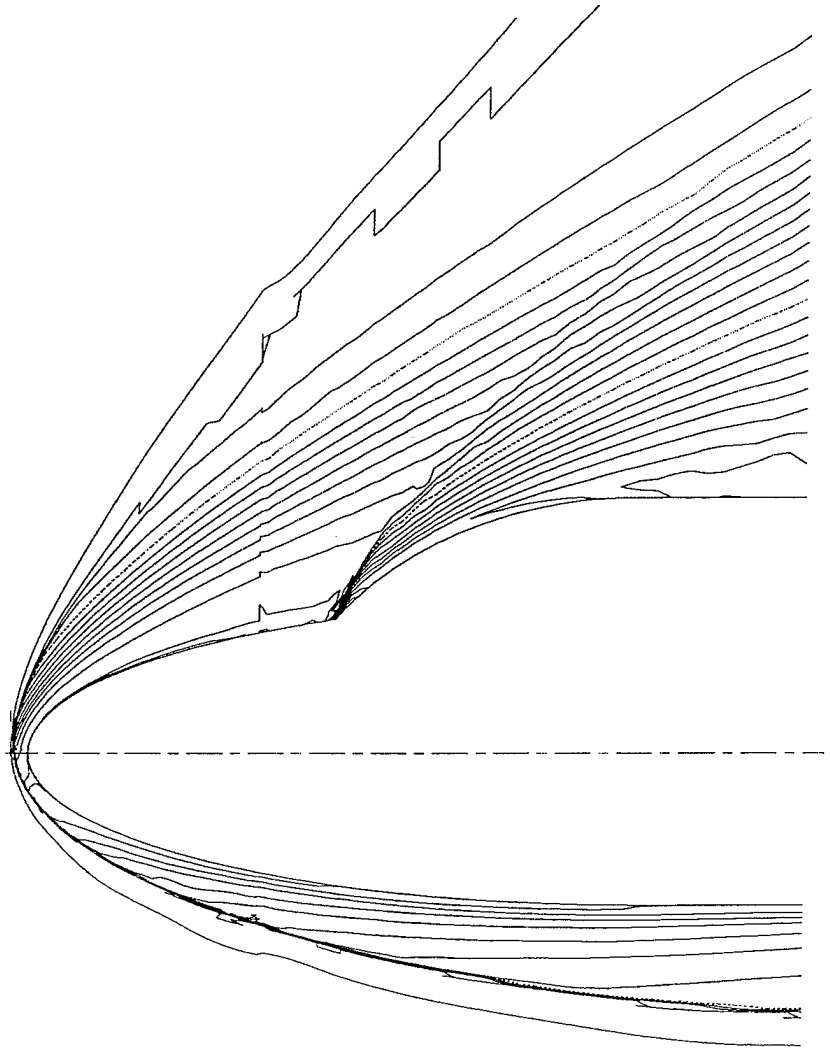

Figure 10. Problem 6.1.7, $M_\infty = 8.15$, $\alpha = 30°$. Entropy isovalue contours in the plane $y = 0$ ($\Delta s = 0.5$).

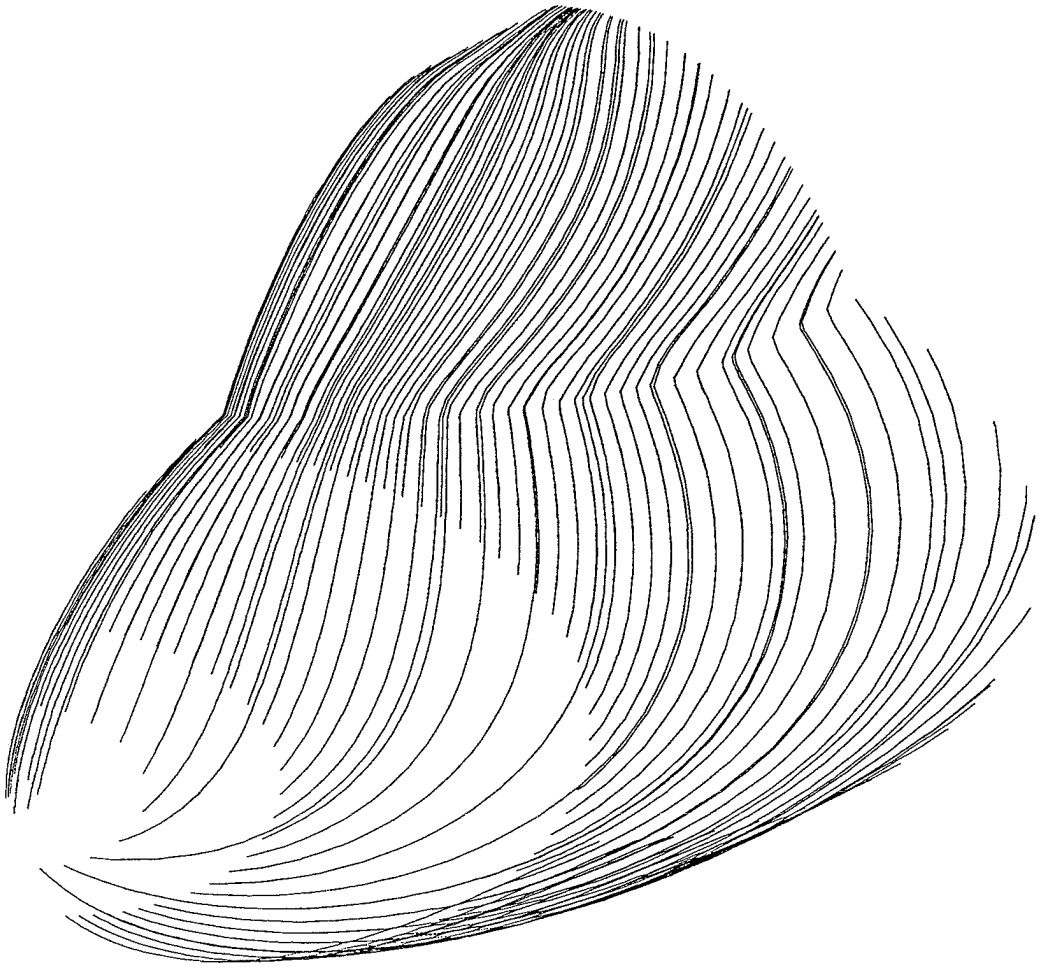

Figure 11. Problem 6.1.7, $M_\infty = 8.15$, $\alpha = 30°$. Side view of the wall streamlines.

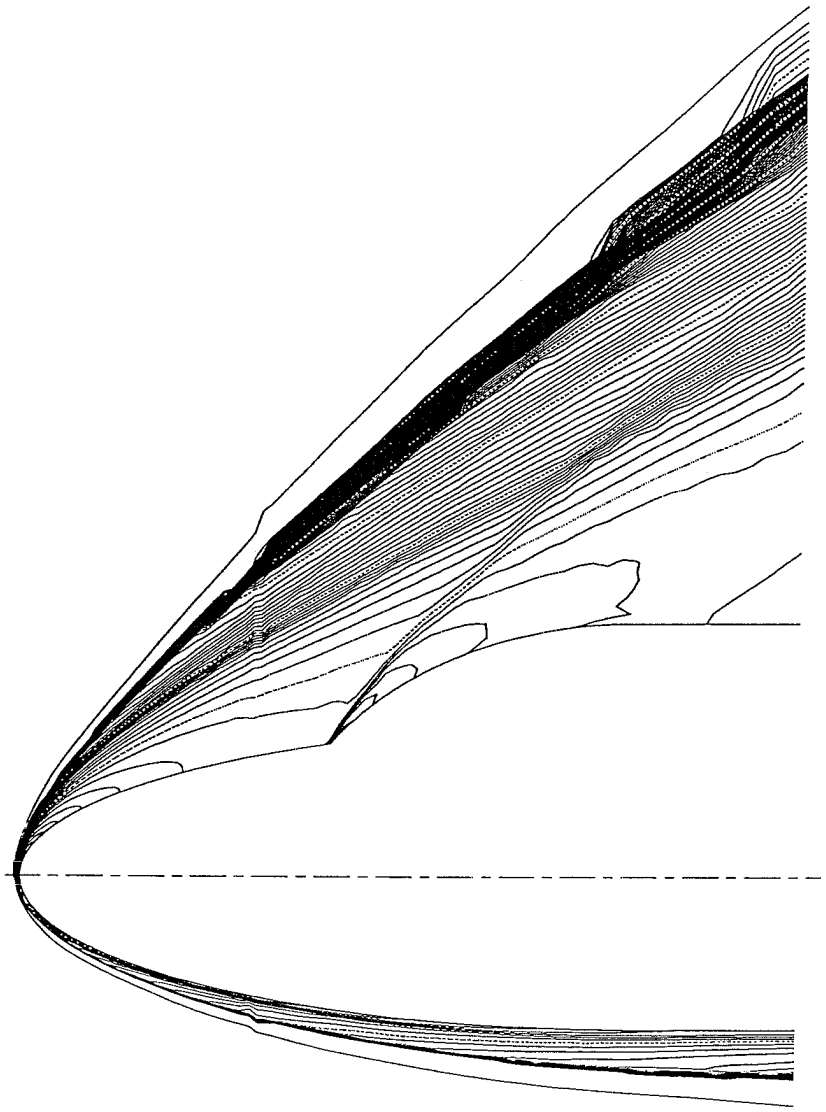

Figure 12. Problem 6.3.9, $M_\infty = 25$, $\alpha = 30°$. Mach number iso-value contours in the plane $y = 0$ ($\Delta m = 0.25$).

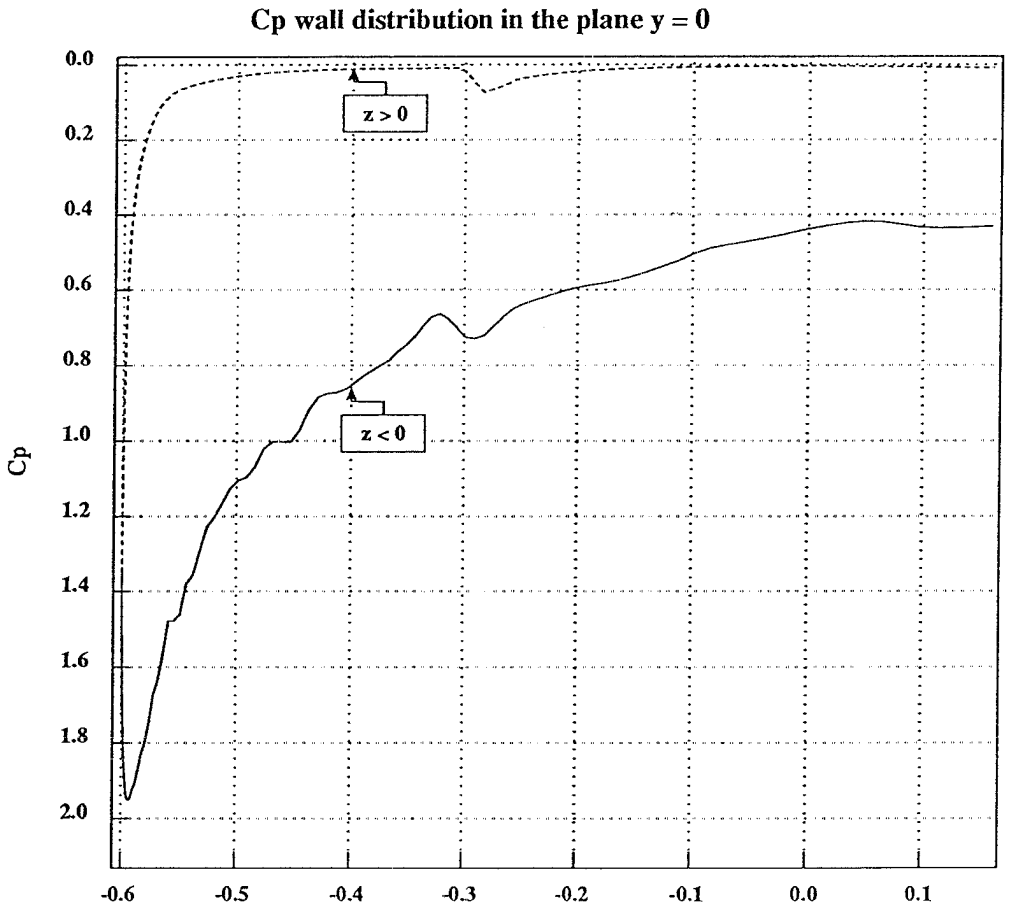

Figure 13. Problem 6.3.9, $M_\infty = 25$, $\alpha = 30°$. Cp wall distribution in the plane y = 0.

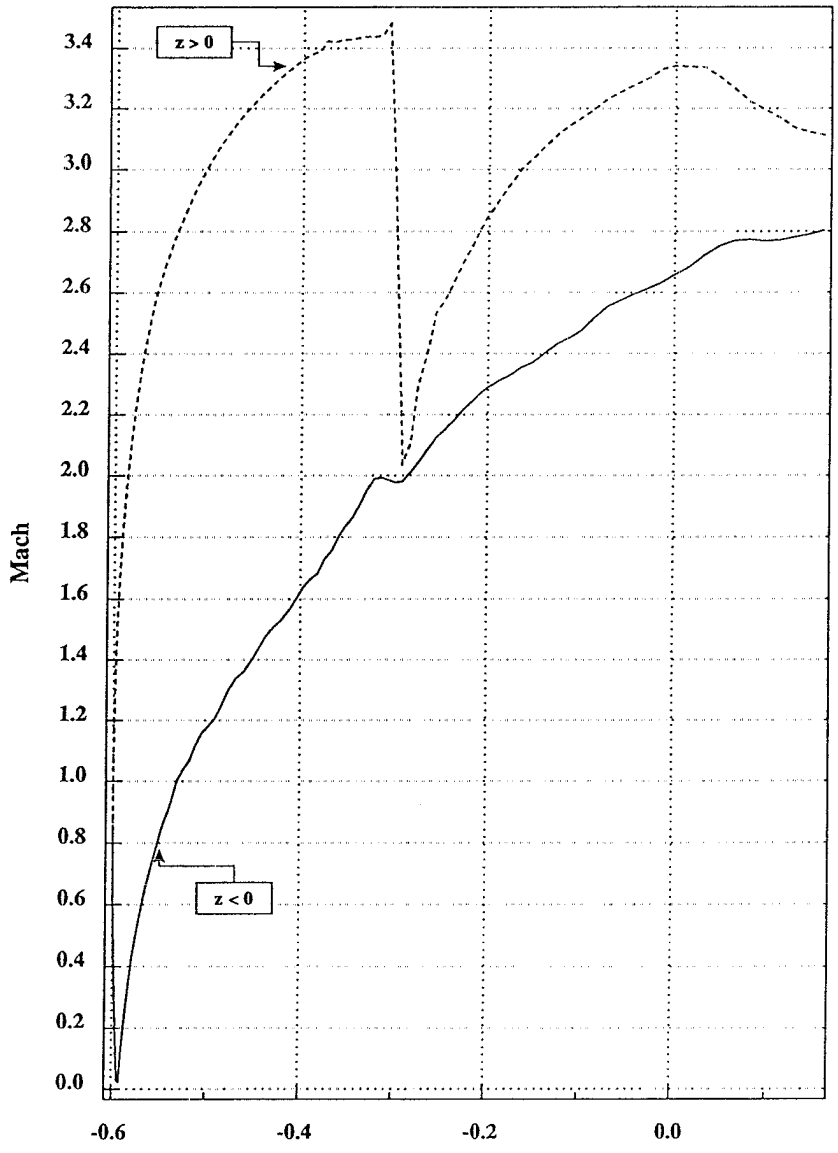

Figure 14. Problem 6.3.9, $M_\infty = 25$, $\alpha = 30°$. Mach number wall distribution in the plane $y = 0$.

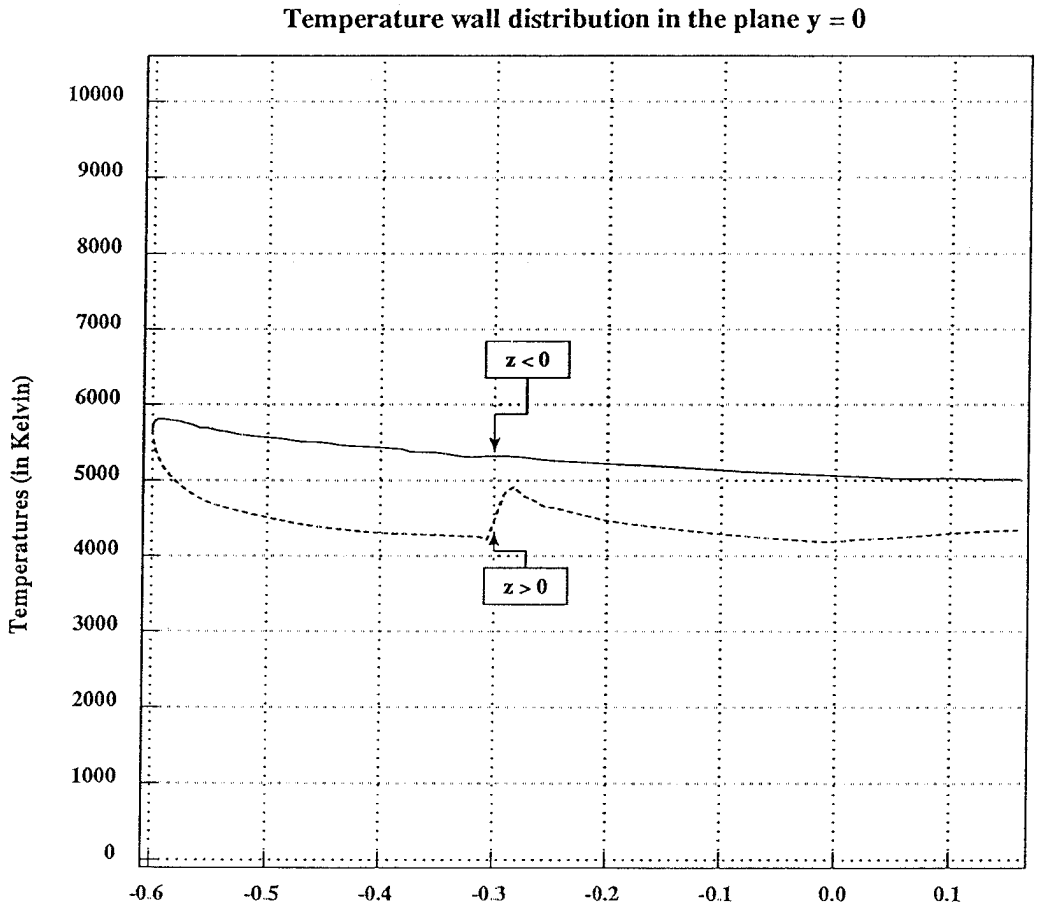

Figure 15. Problem 6.3.9, $M_\infty = 25$, $\alpha = 30°$. Temperature distribution on the body in the plane y = 0.

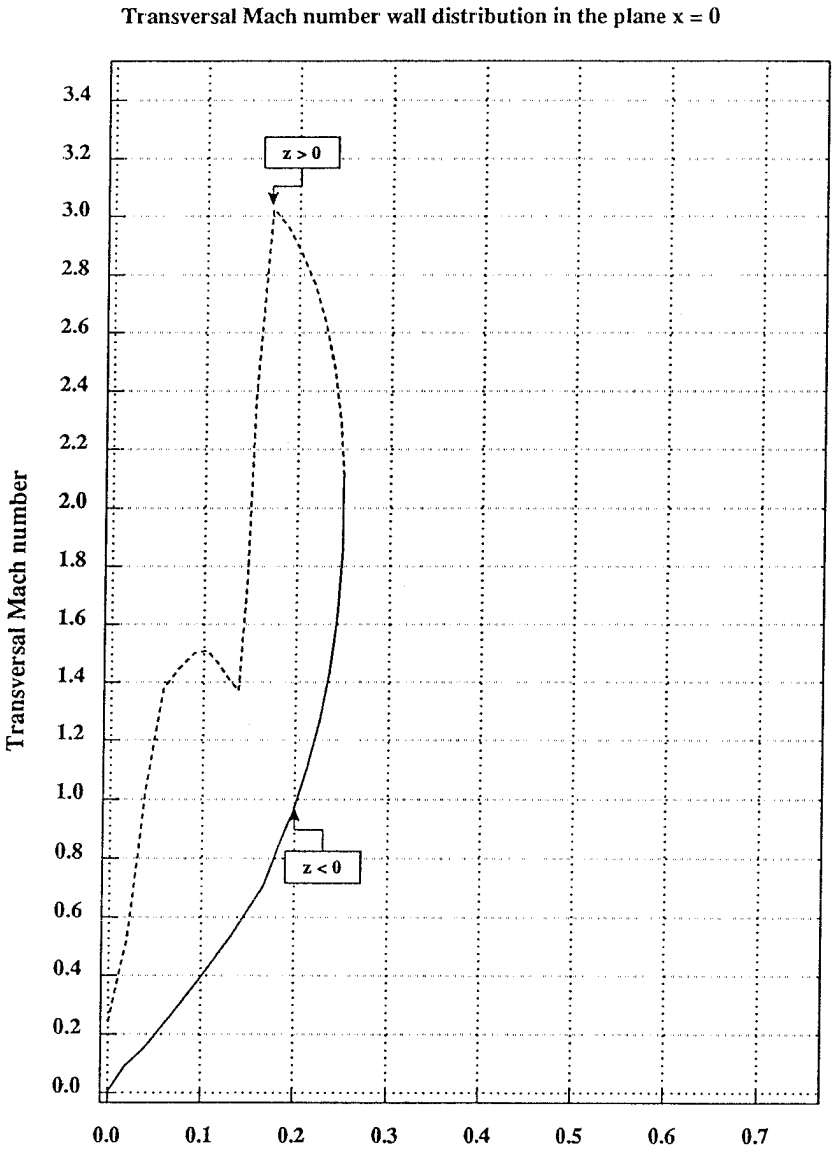

Figure 16. Problem 6.3.9, $M_\infty = 25$, $\alpha = 30°$. Transversal Mach number on the body and in the plane x = 0.

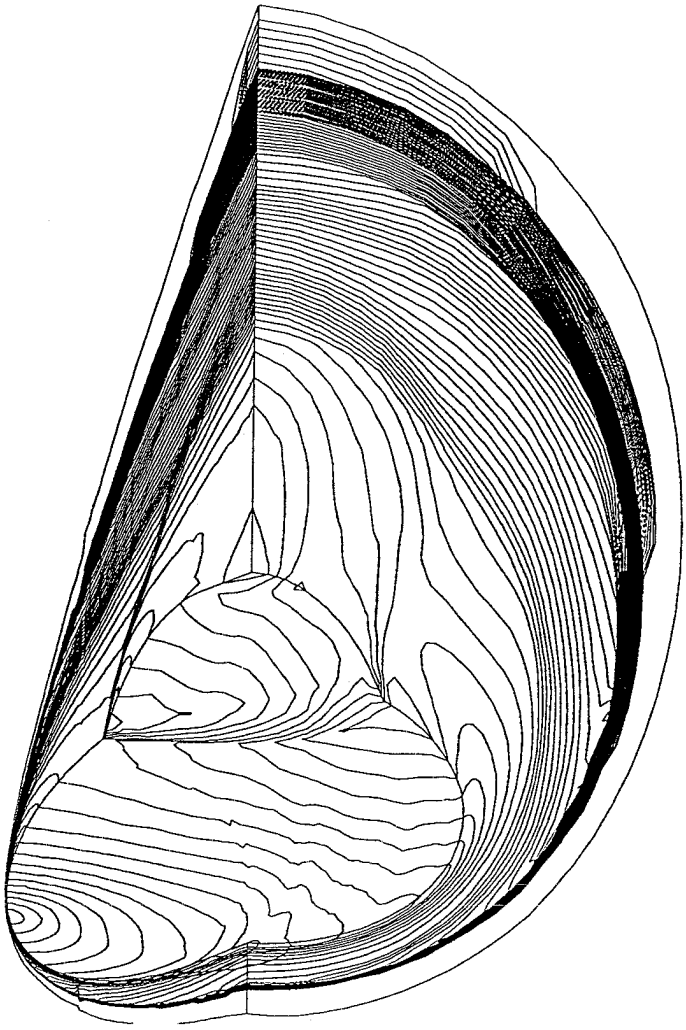

Figure 17. Problem 6.3.9, $M_\infty = 25$, $\alpha = 30°$. Mach number iso-value contours on the body and in the planes $y = 0$ and $x = 0.016$.

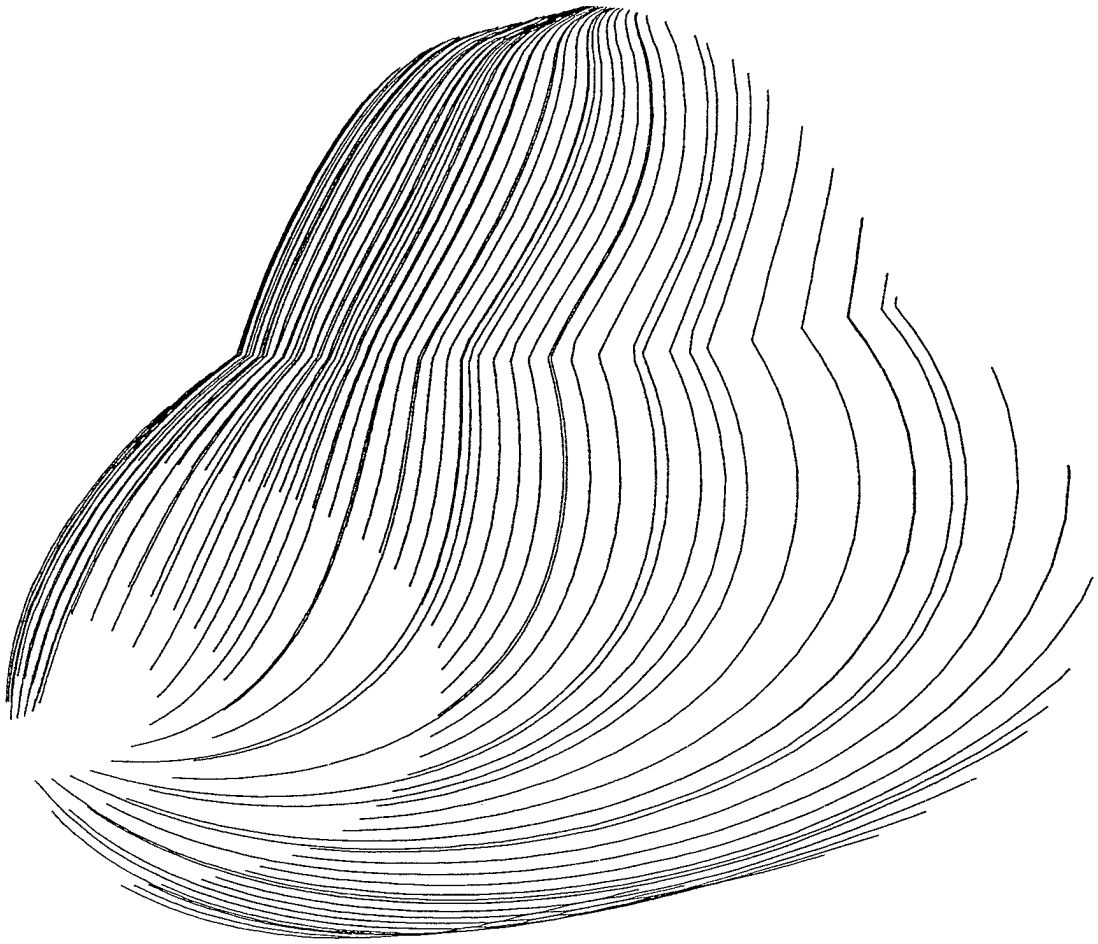

Figure 18. Problem 6.3.9, $M_\infty = 25$, $\alpha = 30°$. Side view of the the wall streamlines.